New Phytologist

Coupled ecohydrology and plant hydraulics modeling predicts ponderosa pine seedling mortality and lower treeline in the US Northern Rocky Mountains

Caelan Simeone[1,6], Marco P. Maneta[1], Zachary A. Holden[2,3], Gerard Sapes[4], Anna Sala[4] and Solomon Z. Dobrowski[5]

[1]Department of Geosciences, University of Montana, Missoula, MT 59812, USA; [2]US Forest Service, Region 1, Missoula, MT 59807, USA; [3]Department of Geography, University of Montana, Missoula, MT 59812, USA; [4]Division of Biological Sciences, Ecology, and Evolution, University of Montana, Missoula, MT 59812, USA; [5]Department of Forest Management, University of Montana, Missoula, MT 59812, USA; [6]Present address: US Geological Survey, New England Water Science Center, Augusta, ME 04330, USA

Author for correspondence:
Caelan Simeone
Tel: +1 406 580 0649
Email: csimeone@usgs.gov

Received: *10 June 2018*
Accepted: *18 September 2018*

New Phytologist (2019) **221:** 1814–1830
doi: 10.1111/nph.15499

Key words: conifer seedlings, ecohydrology, hydraulic conductivity, hydraulic stress, lower treeline, mortality, ponderosa pine (*Pinus ponderosa*).

Summary

- We modeled hydraulic stress in ponderosa pine seedlings at multiple scales to examine its influence on mortality and forest extent at the lower treeline in the northern Rockies.
- We combined a mechanistic ecohydrologic model with a vegetation dynamic stress index incorporating intensity, duration and frequency of hydraulic stress events, to examine mortality from loss of hydraulic conductivity. We calibrated our model using a glasshouse dry-down experiment and tested it using *in situ* monitoring data on seedling mortality from reforestation efforts. We then simulated hydraulic stress and mortality in seedlings within the Bitterroot River watershed of Montana.
- We show that cumulative hydraulic stress, its legacy and its consequences for mortality are predictable and can be modeled at local to landscape scales. We demonstrate that topographic controls on the distribution and availability of water and energy drive spatial patterns of hydraulic stress. Low-elevation, south-facing, nonconvergent locations with limited upslope water subsidies experienced the highest rates of modeled mortality.
- Simulated mortality in seedlings from 2001 to 2015 correlated with the current distribution of forest cover near the lower treeline, suggesting that hydraulic stress limits recruitment and ultimately constrains the low-elevation extent of conifer forests within the region.

Introduction

Forest cover is predicted to decline in the western US in the next century, due in part to increased hydraulic stress associated with climate change (Van Mantgem *et al.*, 2009; Jiang *et al.*, 2013; Hartmann *et al.*, 2015; McDowell *et al.*, 2016). These predictions are consistent with observed shifts in ecosystem composition (Walther *et al.*, 2002; Parmesan & Yohe, 2003) and with increases in the frequency and magnitude of hydraulic stress-induced forest mortality events over the last two decades (Allen *et al.*, 2010, 2015). Increasing air temperatures are extensively documented over much of the western US (Christensen *et al.*, 2007; IPCC, 2015) and compound the effects of water limitations through increased evaporative demand (Weiss *et al.*, 2009; Williams *et al.*, 2013). More frequent drier and warmer periods are expected to impact the distribution of common low-elevation species in the western US, such as ponderosa pine (*Pinus ponderosa*) (Coops *et al.*, 2005; Rehfeldt *et al.*, 2014). These impacts will occur not only through mature tree die-off events (Allen & Breshears, 1998) but also through a decline in the frequency of climatic conditions favorable for seedling establishment, especially along the low-elevation, drier margin of these species' ranges (Rother *et al.*, 2015; Petrie *et al.*, 2016). While recruitment dynamics have been studied extensively at the upper treeline (Smith *et al.*, 2009; Kueppers *et al.*, 2017), less is known about the lower treeline (the forest boundary dictated by water limitations). Loss of seedling recruitment at the lower treeline could dramatically decrease the distribution of forest cover, given the high edge : area ratios of low-elevation forest boundaries. Here, we take an experimental and modeling approach to address whether the distribution of landscape-scale hydraulic stress in seedlings predicts seedling mortality and controls the position of the lower treeline.

Forest demography, composition and distribution are sensitive to recruitment rates of different tree species (Petrie *et al.*, 2016), which in turn are sensitive to hydraulic stress (Savage *et al.*, 1996; Dobrowski *et al.*, 2015). Although the same physical principles drive water transport in seedlings and adult trees, seedlings and saplings are more vulnerable to hydraulic stress-induced mortality than older trees due to a variety of factors, including limited

buffering capacity and less access to deeper groundwater (Harcombe, 1987; Johnson *et al.*, 2011; Bell *et al.*, 2014). Understanding seedling responses to hydraulic stress is essential to assessing the stability of current forest boundaries and to identifying forested regions that are vulnerable to ecosystem transitions (Bell *et al.*, 2014; Petrie *et al.*, 2017).

Important advances in understanding tree mortality have emerged from characterizing the soil–plant–atmosphere continuum (SPAC). Limited soil water supply, particularly under high atmospheric demand, leads to increasingly negative water potentials in the xylem. Low water potentials drive cavitation-induced xylem embolism, reducing plant hydraulic conductivity and impairing a plant's ability to transport water (Tyree & Sperry, 1988; Tyree, 1997; Sperry *et al.*, 1998; Venturas *et al.*, 2017). Large losses of conductivity have been linked to hydraulic stress-induced mortality (Adams *et al.*, 2017; Martínez-Vilalta & Garcia-Forner, 2017). In addition to potential phloem failure (Reinhardt *et al.*, 2015), severe losses of conductivity cause hydraulic failure (McDowell *et al.*, 2008; Sevanto *et al.*, 2014), while more prolonged, less severe periods of hydraulic stress cause both hydraulic impairment and carbohydrate depletion (Moyes *et al.*, 2013; Reinhardt *et al.*, 2015; Adams *et al.*, 2017), leading to cascading system failures (Anderegg *et al.*, 2012). Experimentally determined water potential thresholds of hydraulic impairment (Choat *et al.*, 2012) have been used to map mortality risk using correlative metrics such as temperature and climatic water deficit (Williams *et al.*, 2013; Anderegg *et al.*, 2015a). Alternative studies have used mechanistic models to simulate plant water potential, loss of xylem conductivity and plant carbon status to predict plant responses to drought and mortality (Mackay *et al.*, 2003; Ogée *et al.*, 2003; McDowell *et al.*, 2013; Tai *et al.*, 2017, 2018). To reduce computational costs, mechanistic models are often run over small domains (Tai *et al.*, 2018), are forced with meteorological data that are too coarse to resolve topoclimatatic influences (McDowell *et al.*, 2016), or use terrain indices rather than fully integrated methods of addressing topographic controls on hydrology (Tai *et al.*, 2017). Despite their increased complexity, mechanistic approaches have the advantage of being transferrable across scales and conditions and provide an opportunity for process insight that is not possible with correlative methods.

Despite advances in our understanding of the relationship between water limitations and tree mortality (Sperry *et al.*, 1998; McDowell, 2011; Martínez-Vilalta & Garcia-Forner, 2017; Venturas *et al.*, 2017), our ability to predict landscape-scale hydraulic stress-induced tree mortality remains limited. The linkages between plant hydraulic stress and tree mortality are complex and vary between species and growth stages. These linkages also depend on climate and physical processes that vary at fine spatial scales in regions of complex topography (L. D. L. Anderegg *et al.*, 2013). In addition, varying intensity, duration and frequency of hydraulic stress have been shown to be important in hydraulic stress-induced mortality (Porporato *et al.*, 2001; Mitchell *et al.*, 2013).

Legacy effects of prior drought stress events result from a series of responses that prevent plants from recovering their status (whether in the short or longer term) to that before the stress event once the event has ended (Anderegg *et al.*, 2015b; Pellizzari *et al.*, 2016; Huang *et al.*, 2018; Serra-Maluquer *et al.*, 2018; Wu *et al.*, 2018). For instance, hydraulic deterioration as a result of cavitation fatigue (Hacke *et al.*, 2001) has been shown to limit recovery after drought (L. D. L. Anderegg *et al.*, 2013). Likewise, carbon demand to offset root mortality (Worrall *et al.*, 2008) during drought or to produce new xylem when drought-damaged xylem cannot be repaired (Brodribb *et al.*, 2010) also limit drought recovery. These effects are rarely incorporated in models, which instead use percentage loss of conductivity in the xylem (PLC) at a single point in time or a seasonal mean of PLC to estimate mortality. As a result, we have a limited understanding of how the dynamics of stress duration, intensity and legacy effects drive mortality.

In this study, we develop a mechanistic ecohydrologic model to simulate landscape-scale water and energy exchanges and their influence on plant hydraulic function. We used the model in conjunction with a glasshouse experiment of ponderosa pine seedling mortality to (1) calibrate plant hydraulic parameters and (2) determine the functional dependence of seedling mortality risk on declining xylem hydraulic function. Our approach uses statistics of the mechanistically derived measures of plant stress under the assumption that a sequence of events (periods of stress) of different duration and intensities accumulates plant hydraulic stress-induced fatigue, thus increasing the likelihood of mortality. We tested the model on seedling mortality data from US Forest Service (USFS) reforestation efforts. We then applied the model in a semiarid watershed in western Montana and compared the spatial distribution of simulated seedling hydraulic stress with forest cover with the goal of understanding hydroclimatic limits on tree regeneration. Specifically, we investigate how topographic controls on water and energy fluxes drive seedling exposure to hydraulic stress, and how the spatial distribution of these stresses may drive vulnerability of the lower treeline at landscape scales.

Materials and Methods

Ecohydrologic model

We extend an ecohydrologic model, Ech2o (Maneta & Silverman, 2013), to investigate the impact of the redistribution of water and energy at the landscape scale on plant xylem hydraulic stress. Ech2o is a spatially distributed, mechanistic model that couples a two-layer vertical solution of the energy balance, a water balance with lateral and vertical water redistribution based on the kinematic wave, and a dynamic vegetation growth scheme. Ech2o has an intermediate level of complexity compared to other ecohydrologic models, bridging a gap between catchment hydrology models and comprehensive land surface models that simulate energy, water and biotic interactions within the critical zone. Because of its relatively parsimonious design, Ech2o can run efficiently over large domains at relatively high spatial and temporal resolutions. We coupled Ech2o with a plant hydraulics model (Ech2o-SPAC) to simulate dynamic SPAC processes in a fully integrated manner across landscape gradients of energy and water.

Maneta & Silverman (2013), Lozano-Parra *et al.* (2014) and Kuppel *et al.* (2018) comprehensively describe Ech2o. We provide an overview of the processes it incorporates in Supporting Information Methods S1. Extensions and developments specific for this research including the SPAC formulation and changes to the soil hydrology, stomatal resistance and channel routing processes are described in the next section and in Methods S1 and S2.

Plant hydraulics component

Water transport through the SPAC is a function of water potential gradients within the xylem according to the cohesion–tension theory (Sperry *et al.*, 1998). Cavitation-induced embolisms occur when steep tension gradients between soil and the atmosphere along the SPAC overcome the strength of the water column at nucleation points (Tyree, 1997; Venturas *et al.*, 2017). These events reduce the plant's capacity to transport water and at high rates lead to hydraulic failure and death. Our model simulates the tension gradient driving water lift by solving SPAC transfers between a soil–root node and a canopy–atmosphere node using a formulation similar to that of Daly *et al.* (2004). The SPAC is simulated with a system of four nonlinear equations (soil water balance, soil water potential energy, plant water flux and plant water potential balance, and canopy energy balance) with four unknowns (plant-available soil moisture θ_r, soil water potential ψ_s, leaf water potential ψ_{leaf} and canopy temperature T_c). The equations are solved simultaneously at 3-h time steps for each vegetation type in every cell of the modeling domain using an iterative Newton–Raphson scheme (see Eqn S1 in Methods S2 for details). The solution of the SPAC equations produces, among other things, time series of leaf water potential that are used to determine loss of whole plant conductivity in each cell.

Loss of conductivity depends on midday leaf water potential and is used as a proxy for stress. The fraction of conductivity lost to embolism (referred to as PLC to follow common nomenclature) is:

$$\mathrm{PLC} = 1 - e^{-(-\psi_{leaf}/b)^c}, \qquad \text{Eqn 1}$$

where ψ_{leaf} is leaf water potential (LWP) and b and c are experimental values from a Weibull vulnerability curve: b is the LWP value mathematically corresponding to 63% PLC, and c controls the shape and slope of the function (Sperry *et al.*, 1998; Hubbard *et al.*, 2001) (Notes S1).

Dynamic stress index

To transition from an instantaneous measurement of stress (PLC) to a probabilistic prediction of mortality, we adapt a statistical framework based on the dynamic stress index (DSI, $\bar{\theta}$) presented by Porporato *et al.* (2001). The original DSI framework assumes that hydraulic stress in vegetation begins at the volumetric water content (VWC) in the soil at which incipient stomatal closure occurs. Static stress reaches a maximum at the VWC at which stomata completely close. Static stress is the basis for a dynamic measurement of vegetation stress that incorporates the mean intensity, duration and frequency of periods of soil moisture deficit. In our implementation, we substitute PLC for VWC to calculate DSI. PLC subsumes tension dynamics in the soil and xylem and includes variable hydraulic architecture and response to the onset of water deficit. We interpret DSI as the integrated probability of tree mortality at a location.

To calculate DSI we first calculate a static stress index, $\zeta(t)$. When PLC surpasses an initial threshold (PLC_{init}), stress increases until a maximum threshold of stress (PLC_{crit}). A piecewise function calculates the static stress index:

$$\zeta(t) = \begin{cases} 0, & \text{if } \mathrm{PLC}(t) < \mathrm{PLC}_{init} \\ \frac{\mathrm{PLC}_{init} - \mathrm{PLC}(t)}{\mathrm{PLC}_{init} - \mathrm{PLC}_{crit}} & \text{if } \mathrm{PLC}_{init} < \mathrm{PLC}(t) < \mathrm{PLC}_{crit} \\ 1, & \text{if } \mathrm{PLC}(t) > \mathrm{PLC}_{crit}. \end{cases} \qquad \text{Eqn 2}$$

We calculate the mean weighted stress ($\bar{\zeta}'$) during the growing season as the accumulated static stress during the growing season:

$$\bar{\zeta}' = \frac{\int_0^1 (\zeta f(\zeta) d\zeta) + P(1)}{P(\mathrm{PLC}_{init})}, \qquad \text{Eqn 3}$$

where $P(1)$ is the probability (i.e. frequency) that static stress exceeds the maximum threshold (PLC_{crit}). The integral accounts for periods when stress is between the initial (PLC_{init}) and maximum (PLC_{crit}) thresholds. $P(\mathrm{PLC}_{init})$ is the probability of exceeding the minimum threshold.

The mean weighted hydraulic stress ($\bar{\zeta}'$) accounts for the mean intensity of stress during periods of stress but lacks direct information on either the duration or frequency of stress, both of which impact plant response. Once $\bar{\zeta}'$ is calculated, information on the frequency and duration of events is included in the dynamic stress index ($\bar{\theta}$), which is constrained between zero and one and represents the probability of mortality:

$$\bar{\theta} = \begin{cases} \left(\frac{\bar{\zeta}' \overline{T}_{\mathrm{PLC}}}{k T_{seas}}\right)^{\overline{n}_{\mathrm{PLC}}^{r}}, & \text{if } \bar{\zeta}' \overline{T}_{\mathrm{PLC}} < k T_{seas} \\ 1, & \text{otherwise} \end{cases} \qquad \text{Eqn 4}$$

where T_{seas} is the length of the growing season, determined by the number of days with modeled soil temperature above 5°C (Bailey & Harrington, 2006; Beedlow *et al.*, 2013), using the average temperature modeled through the full soil column. $\overline{T}_{\mathrm{PLC}}$ and $\overline{n}_{\mathrm{PLC}}$ are, respectively, the average length and frequency of stress events where hydraulic impairment over the level of PLC_{init} occurs. Parameter k is a constant for plant resistance to hydraulic stress. Parameter r represents legacy effects from hydraulic stress (Porporato *et al.*, 2001). It does so by incorporating the frequency by which a given stress event leads to PLC exceeding PLC_{init}, the mean hydraulic stress during that stress event (mean average of hydraulic function) and the overall cumulative result of successive stress events over time as a function of how often and for how long they occur. While r does not account for the

specific mechanisms involved (e.g. hydraulic fatigue, inability to refill embolized xylem, root mortality), it does account for their combined negative effect on hydraulic function. When r is zero, the exponent in Eqn 4 is one and the effect of the frequency of stress events ($\bar{n}_{PLC}$) is eliminated, representing the case when plants fully recover after a stress event, in which case the frequency of stress periods is irrelevant. Higher values of r introduce information about the frequency of stress events $\bar{n}_{PLC}$ in the calculation of $\bar{\theta}$, allowing the index to capture the partial recovery and accumulation of damage in the vascular and photosynthetic systems from frequent stressful events.

Glasshouse dataset used for calibration

We used data from a glasshouse experiment conducted at the University of Montana to calibrate our model parameters for predictions of both physiological signals of stress and seedling mortality rates under hydraulic stress. This experiment exposed 250, 1-yr-old ponderosa pine seedlings of the genetically distinct Northern Rocky Mountain race (Potter *et al.*, 2013) to three successive dry-down cycles followed by re-watering to pre-condition seedlings before a final dry-down leading to death. Periodically during the dry-down, subsets of 30 randomly selected seedlings were re-watered and their mortality (i.e. probability of mortality of the population) was determined after at least 1 month based on foliage browning, completely desiccated phloem and no signs of recovery. At each sampling time, an independent subset of five seedlings was sampled to assess physiological status (including transpiration and LWP) followed by destructive measurements to determine PLC. Such a design based on the point of no return (when seedlings can no longer recover) allowed us to estimate the population's probability of mortality over time and relate it to the mean physiological status of seedlings at that point. LWP and PLC values were used to fit a Weibull vulnerability curve for the seedlings. We measured soil VWC with a 30 min sampling resolution using three randomly selected pots instrumented with 5TE soil sensors (Meter Inc., Pullman, WA, USA) placed at the same soil depth.

Calibration approach

The model represented the glasshouse as a 3×3 pixel flat domain to simulate four dry-downs. Hourly measurements from the glasshouse of temperature (Vaisala HMP35C; Vantaa, Finland), solar radiation (Licor 200X; Lincoln, NE, USA), and relative humidity (Vaisala HMP35C) provide atmospheric boundary conditions. We estimated longwave radiation from measured air temperature using the Stefan–Boltzmann equation (emissivity = 0.95). To prevent zero modeled transpiration during measured periods of zero wind speed we limited the minimum wind speed used in the model to 0.25($m\ s^{-1}$). Plant watering schedules and amounts were simulated as precipitation inputs. Fig. S1 presents the climatic boundary conditions of the glasshouse experiment. Noncalibrated plant and soil input parameters were directly measured in the glasshouse, extracted from the literature when a direct measurement was not available, or estimated from previous Ech2o runs when neither was available (Tables S1, S2). We used a Monte Carlo Markov chain (MCMC) approach for calibration as implemented in the package PYMC3 (Salvatier *et al.*, 2016) using the Metropolis-Hastings algorithm (Hastings, 1970) to infer posterior model parameter distributions and the Gibbs-Step-Slice-Sampler algorithm (Geman & Geman, 1984) to infer observation errors, modeled as a latent variable of the likelihood function. We divided the calibration into two steps. In the first, we calibrated Ech2o-SPAC to simulate the physiological response of seedlings to the dry-down in the glasshouse. We included a group of the most sensitive parameters in the calibration (Table S3). We performed 5500 MCMC model iterations sampling the parameter space and estimating our posterior distribution. We matched measured VWC, transpiration and LWP with multiple objective calibration. In the second step, we calibrated three variables in the DSI framework (PLC_{init}, PLC_{crit} and k) against the observed probability of mortality from the glasshouse. For each of our 5500 MCMC model iterations, we took the LWP time series from an Ech2o-SPAC run with the mean calibrated parameters and applied the DSI framework to that time series. We held r at 0.5 (see Porporato *et al.*, 2001) during this calibration because there was only one stress-inducing event in the glasshouse, which prevented us from examining hydraulic stress legacy effects on plants.

Northern Rockies seedling survival data

At the stand scale, we used data on seedling survival rates from the USFS Region 1 reforestation program. Following timber harvest or disturbance, 1–3-yr-old nursery-grown seedlings were planted to facilitate reforestation. At these sites, stake rows of seedlings were monitored at 1 and 3 yr after planting to assess the fraction of seedlings that experienced mortality. Most of the stake row data represented 2–3-yr-old seedlings. Consequently, from the full dataset, we extracted data for 29 sites in which 1-yr-old bare-root seedlings were planted (the closest stock type to our glasshouse calibration) for ponderosa pine, Douglas fir (*Pseudotsuga menziesii*) and western larch (*Larix occidentalis*) (Fig. 1). Each of these sites had 30 or more seedlings in their stake row (mean = 71, SD = 38). These stake row sites span a range of elevations (mean = 1534 m, SD = 341 m), annual precipitation (mean = 0.72 m, SD = 0.19 m) and mean annual temperature (mean = 9.8°C, SD = 2.5°C).

We ran Ech2o-SPAC at a 3 h time-step at each reforestation site from 2001 to 2015, simulating a center target cell with a buffer one cell wide (nine cells in total) to facilitate lateral routing of water. Ech2o-SPAC requires five soil properties as spatial input: soil depth, porosity, saturated hydrologic conductivity, Brook–Corey pore size distribution index and albedo. These values were extracted from the US Department of Agriculture Soil Survey Geographic Database (SSURGO). For areas where SSURGO data were unavailable, we developed models for each soil property layer to estimate missing soil values following methods described by Landguth *et al.* (2017). Changes in parameters from the glasshouse are presented in Tables S1 and S2. Weather

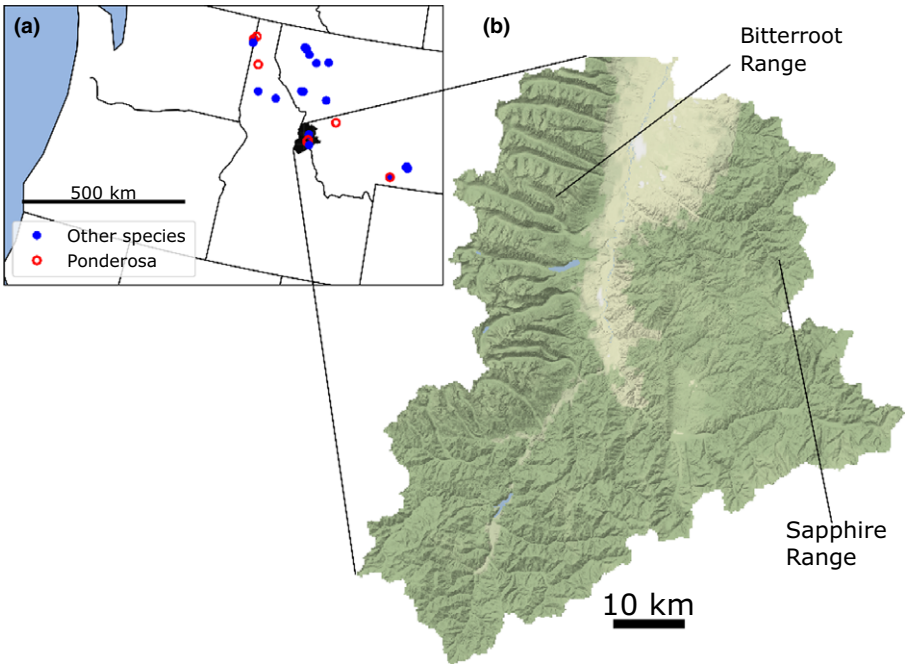

Fig. 1 (a) Location of US Forest Service stake row sites and Bitterroot watershed. *Pinus ponderosa* are in red, and other species in blue. The black outline is the Bitterroot Watershed. (b) The southern portion of the Bitterroot Watershed.

inputs required to run Ech2o-SPAC include minimum and maximum temperature and relative humidity, shortwave and longwave radiation, precipitation and wind speed. Daily gridded temperature, relative humidity and solar radiation inputs for simulations at each stake row point were extracted from 250 m grids (Holden *et al.*, 2018). Daily precipitation data were extracted from 4 km PRISM data and resampled to 250 m resolution by bilinear interpolation (Daly *et al.*, 2008). Wind speed data were extracted from daily mean wind speed grids from the North American regional reanalysis data (Mesinger *et al.*, 2006). We downscaled daily weather data values to 3 h values using time of sunrise and sunset and sine functions adapted from the CHILLR library (Luedeling, 2018) in R (R Core Team, 2010). Mean daily wind speed was used at each 3 h time step, and total daily precipitation was distributed evenly across each 3 h period. We converted the Ech2o-SPAC time series of LWP to PLC using Eqn 1, then calculated the probability of mortality using the DSI framework (Eqns 2–4).

Evaluation of the low-elevation treeline

To evaluate whether model predictions of seedling mortality from hydraulic stress correspond to the current distribution of the lower treeline, we ran Ech2o-SPAC at the landscape scale in the Bitterroot River watershed (8th code HUC 17010205) in western Montana, USA, at a 3 h time step from 2001 to 2015 (Fig. 1). Forest managers report widespread seedling mortality in this area following reforestation efforts (S. Fox, USFS, pers. comm.). The simulation domain covers 4728 km^2 (75 642 250 m grid cells) and spans elevations from 1033 to 3060 m. The watershed encompasses the southern portion of the Bitterroot Mountains to the west; this range is the easternmost portion of the Idaho Batholith and is formerly glaciated (Alden, 1953). The lower elevation Sapphire range (part of the Sapphire Block) is on the east side of the Bitterroot watershed and is primarily underlain by Belt Supergroup lithology. The Sapphire Range has lower overall slopes and thicker and more extensive soil cover than the steeper, more bedrock-dominated Bitterroot Mountains (Benjaram & Dixon, 2015). Weather systems primarily move from west to east, resulting in higher precipitation in the highest elevation portions of the Bitterroot Mountains and progressively lower moisture to the east. Grasslands transitioning into ponderosa pine-dominated forests make up drier low-elevation portions of the watershed.

We ran Ech2o-SPAC in the watershed using vegetation parameters derived from the glasshouse calibration experiment. For vegetation inputs into the model, we assumed a uniform planting of seedlings with a leaf area index of 0.27 m^2 m^{-2} (value from the glasshouse) to examine the potential DSI of newly recruited seedlings assuming unforested terrain. Inputs were the same as for the stake row analysis, with increased effective soil conductivity (Table S1) to better reflect regional hydrology as measured by the hydrograph (Fig. S2).

We evaluated landscape topographic patterns of DSI using terrain indices derived from the US Geological Survey National Elevation Dataset. We focused on examining how elevation, aspect and topographic convergence, three metrics demonstrated to influence ecohydrology, impact the spatial distributions of hydraulic stress (Allen & Breshears, 1998; Worrall *et al.*, 2008; Hawthorne & Miniat, 2018). To measure convergence, we calculated the topographic position index (TPI; Weiss, 2001), where zero is planar, more negative values are more convergent and more positive values are more divergent. We extracted values from gridded datasets of mean solar radiation (W m^{-2}, indicative of aspect), mean daily maximum temperature (°C), mean annual precipitation (m) and peak snow depth (m). Similarly, we

extracted values of key ecohydrologic variables across the watershed, including vapor pressure deficit (VPD) , VWC and DSI. VPD (kPa, indicative of atmospheric demand) is the summer mean daily minimum value. VWC ($m^3\ m^{-3}$, indicative of water supply) is the mean summer value in the rooting zone (top 40 cm of soil).

We compared spatial maps of simulated hydraulic stress (DSI) with two existing forest cover products to examine the relationship between projected seedling mortality and forest distribution. We used the 250 m Moderate Resolution Imaging Spectroradiometer (MODIS) vegetation continuous field percentage canopy cover product for the year 2015 (DiMiceli *et al.*, 2011) and the LANDFIRE program canopy height product (Landfire, aggregated from 30 to 250 m) forest cover maps for 2015 (Rollins, 2009). All maps were initially analyzed visually to assess trends in the distribution of stress across the landscape. DSI was overlaid on each variable and split into 100 bins based on the mapped variable value. The median DSI value of each bin was plotted along with an envelope of the 10th and 90th percentiles. To further examine the impact of lateral routing and convergence we partitioned points in the landscape into convergent ($TPI < -50$), planar ($-50 \leq TPI \leq 50$) and divergent ($TPI > 50$) locations. We plotted DSI binned across atmospheric variables to examine how convergence influences the relationship between plant stress and atmospheric drivers. We examined the relationships between DSI, TPI, elevation, solar radiation, VWC and VPD graphically.

To examine the relationship between DSI for seedlings and forest distribution, we classified MODIS forest cover as forest/no forest at a threshold of 10%, below which an area was deemed

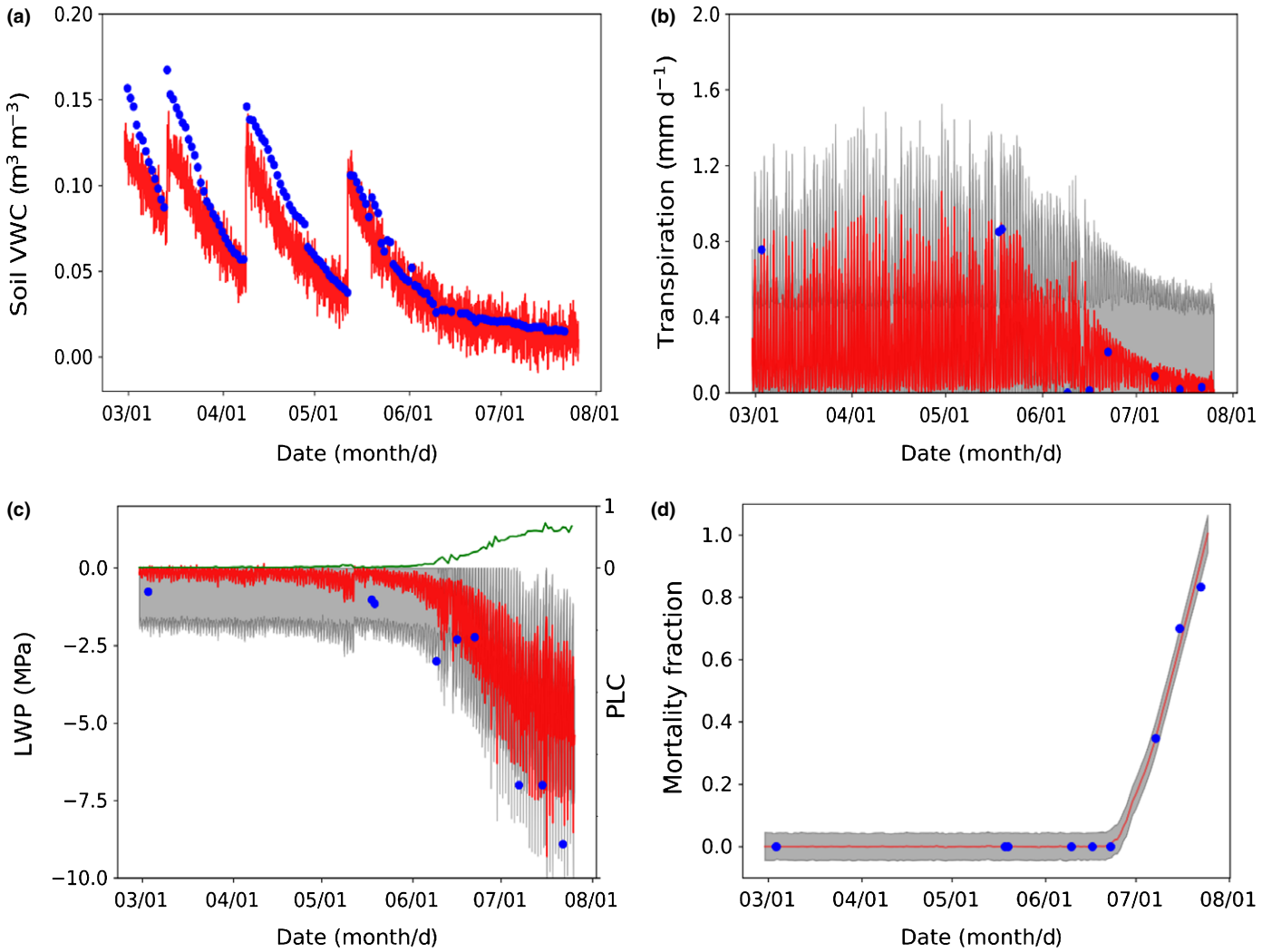

Fig. 2 Modeled and observed fits for the glasshouse experiment on ponderosa pine seedlings: (a) soil volumetric water content (VWC) ($R^2 = 0.94$, $P < 0.01$, slope = 0.79), (b) transpiration ($R^2 = 0.74$, $P < 0.01$, slope = 0.74), (c) leaf water potential (LWP) ($R^2 = 0.94$, $P < 0.01$, slope = 0.98) and (d) fraction of mortality (DSI) ($R^2 = 0.99$, $P < 0.01$, slope = 1.04). Modeled values (red) are timeseries values with intervals of 1 h. Observed values (blue) are point measurements. For VWC the interval is once per day. For other variables, the samples are taken throughout the experiment when destructive sampling occurred. Gray shaded areas represent the central 60% of the modeled Monte Carlo distribution. In (c) the green line shows the modeled percentage loss of conductivity (PLC) that results from the corresponding LWP values. The calibrated fits for the DSI calibration (d) were 0.26 PLC for the onset of stress (PLC_{init}), 0.55 PLC for critical stress (PLC_{crit}) and a resistance value (k) of 0.17.

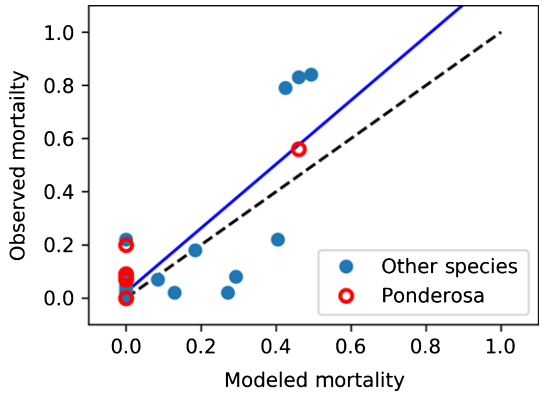

Fig. 3 Modeled vs observed mortality for 1-yr-old bare-root seedlings (ponderosa pine, Douglas fir and western larch) from US Forest Service stake row data. $R^2 = 0.69$. For the best fit line: slope = 1.20, intercept = 0.02. $P < 0.01$. $n = 29$. The dashed line represents the 1 : 1 line between the two variables.

nonforested. Landfire locations with canopy were classified as forested. We classified DSI values as supporting/not supporting regeneration using a threshold value. To determine the proper threshold we calculated minimum, median, mean and maximum DSI between 2001 and 2015 and sampled a range of DSI values (0–1). We then evaluated the agreement between classified DSI and current forest cover maps by calculating the area under the receiver-operator curve (AUC) (Hanley & McNeil, 1982) and Cohen's Kappa statistics (Cohen, 1960) (Notes S2) for the full watershed and for the Skalkaho Creek catchment, a subbasin in the Sapphire Range.

Results

Calibration of the SPAC response

Ech2o-SPAC effectively simulated the observed VWC, transpiration, LWP and mortality response of ponderosa seedlings in our glasshouse dry-down experiment (Fig. 2). Predicted VWC matched the observations for the three initial soil dry-downs and the major mortality-inducing hydraulic stress event (Fig. 2a). Ech2o-SPAC slightly underestimated VWC at or above field capacity, but the match was precise at low VWC, which is critical for predicting stress (Fig. 2a). Transpiration suppression and a steep decline in LWP were observed only after VWC declined in the final dry-down period leading to death (Fig. 2b,c), indicating that Ech2o-SPAC properly captured the onset of high hydraulic stress. Increases in mortality lagged behind indicators of increased stress (Fig. 2d). Hydraulic stress conditions exemplified by low VWC first reduced levels of transpiration, followed by LWP. Low values of LWP were accumulated for a period before plant mortality began, demonstrating the nonlinear threshold behavior captured by Eqn 2. Through calibration of the DSI framework, we found that stress began to accumulate at a PLC (PLC_{init}) of 0.26. The critical level of PLC (PLC_{crit}) and the parameter k were found to be 0.55 and 0.17, respectively (Fig. S3). This indicates that 100% mortality would occur in a population of similar ponderosa pine seedlings exposed to a PLC of 0.55 during 17% of the growing season. Full calibration results are in Tables S3 and S4.

Stake row seedling analysis

Based on the glasshouse calibration, Ech2o-SPAC effectively simulated mortality of 1-yr-old bare-root seedlings of ponderosa pine, Douglas fir and western larch planted in previously disturbed areas (Fig. 3; $r^2 = 0.69$, $P < 0.01$) (Notes S3). The trend of the best fit has a slope of 1.20, and an intercept of 0.02 with a slight underestimation of mortality (modeled mean mortality = 0.11, observed mean mortality = 0.16). This underestimation may be because observed mortality includes all forms of mortality, while modeled mortality only follows hydraulic stress. The fit demonstrates the model's skill moving from the glasshouse to the landscape while incorporating heterogeneous physical and climatic processes.

Hydraulic stress-induced mortality at the landscape scale

When Ech2o-SPAC was fully distributed across the Bitterroot watershed, topography (Fig. 4a,b) strongly influenced the distribution of energetic demand (Fig. 4c,d,g) and water supply (Fig. 4e,f,h). Energy inputs were dominated by elevation (Fig. 4d) and aspect (Fig. 4c), where atmospheric demands decreased with elevation and increased on south-facing slopes (Fig. 4g). Precipitation also increased with elevation (Fig. 4e), although this pattern differed from plant-available soil moisture (Fig. 4h). Elevation and terrain convergence both controlled plant-available soil moisture (Fig. 4b,h). Hydrologic routing concentrated water in convergent locations while draining other positions.

The distribution of dynamic stress in seedlings (Fig. 5) depended on topography (Fig. 6a,b) through the controls that the latter exerts on energetic demand and water supply (Fig. 6c–h). In general, DSI decreased with elevation (Fig. 6a) but varied with convergence and aspect, which distribute lateral routing of water and incoming solar radiation inputs, respectively (Figs 6b,c, 7a,b). Median DSI was near zero in highly convergent zones and increased sharply beyond a TPI convergence threshold (*c.* −50) (Figs 6b, 7a). DSI increased with solar radiation, but not linearly (Figs 6c, 7b). VWC appeared to be the dominant influence on DSI (Figs 6h, 7c) but atmospheric demand influenced DSI at sites with low water availability (Figs 6g, 7c). Additionally, soil VWC did not reach extremely low values (corresponding to high DSI values) without co-occurring large values of VPD (high atmospheric demand for water). Forest cover showed a clear inverse relationship with DSI in regions with sparse forest coverage, but the strength of this relationship decreased once forest cover exceeded 10% (Fig. 6i). Planar areas showed similar relationships between DSI and atmospheric variables as did landscape on a whole (Fig. 8). DSI was more coupled to atmospheric drivers in divergent areas but decoupled in convergent areas (Fig. 8).

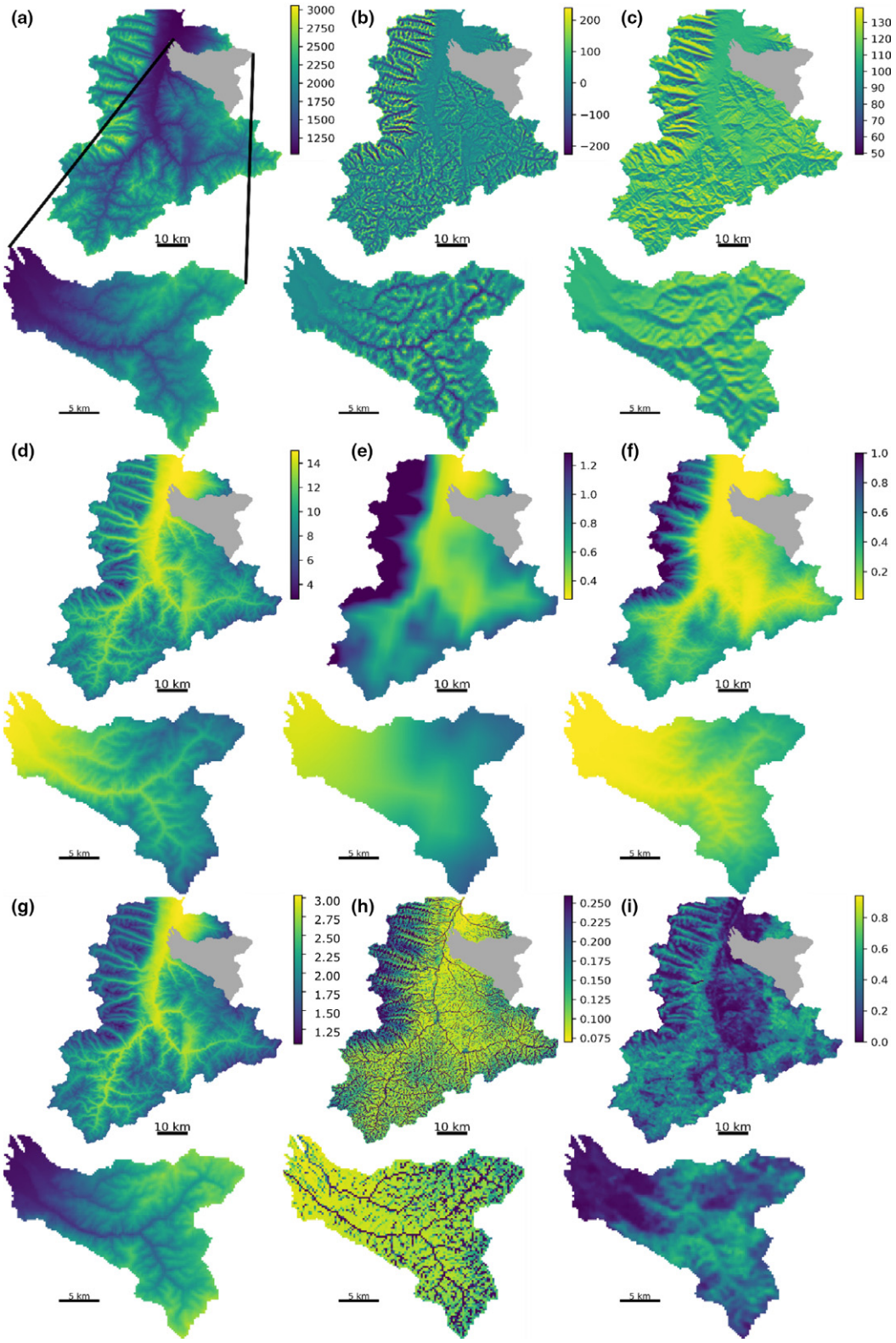

Fig. 4 Maps of physical, climate and ecohydrologic variables for ponderosa pine in the Bitterroot watershed and the Skalkaho subbasin: (a) elevation in the watershed, (b) topographic position index, (c) mean solar radiation, (d) mean maximum daily temperature (°C), (e) total annual precipitation (m), (f) peak annual snow water equivalent (m), (g) summer mean maximum daily vapor pressure deficit (kPa), (h) summer mean volumetric water content in the rooting zone, (i) percentage forest cover derived from MODIS. (f, h) Simulated by Ech2o-SPAC. We calculate statistics in the Skalkaho catchment in addition to the entire Bitterroot watershed because there are relatively fewer confounding factors in the Skalkaho catchment. The Skalkaho catchment additionally spans steep gradients of energy and water in a small enough space to allow for higher resolution visualization of important processes.

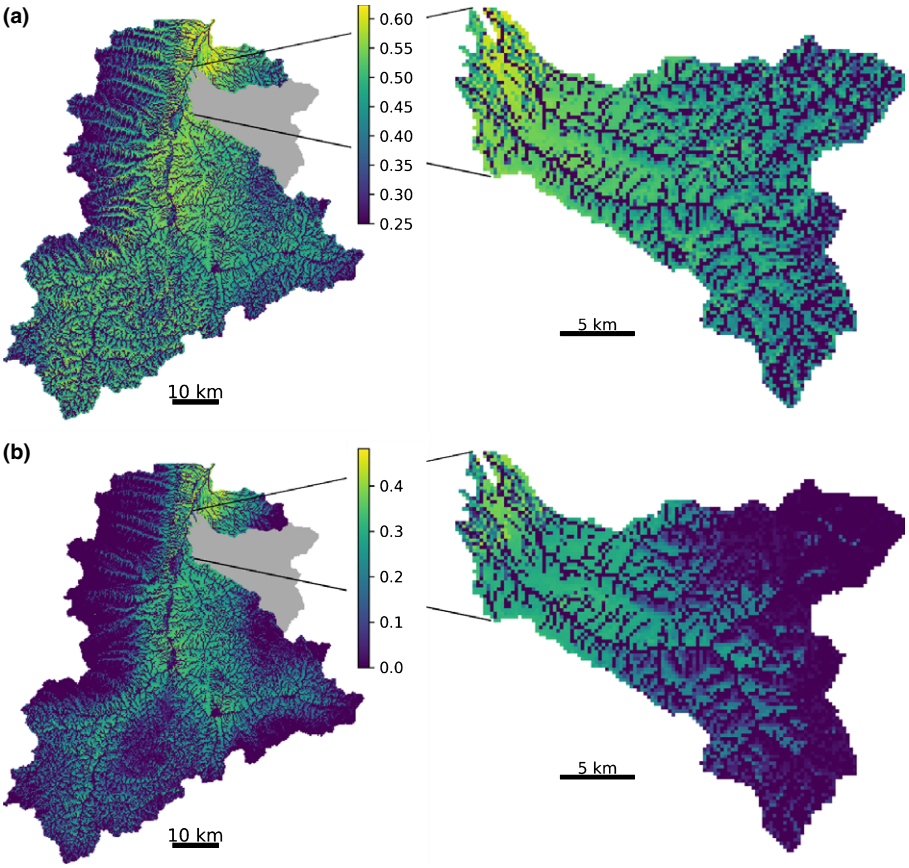

Fig. 5 Dynamic stress index (DSI) of ponderosa pine seedlings for the Bitterroot watershed and the Skalkaho catchment. (a) Mean DSI between 2001 and 2015. (b) Minimum DSI from 2001 to 2015. Warm and cold colors represent higher and lower stresses, respectively.

DSI for seedlings correlates with the presence and absence of low-elevation forest

Our simulations of DSI for ponderosa seedlings from 2001 to 2015 correlated with current forest cover (Fig. 9), supporting the hypothesis that hydraulic failure due to hydraulic stress in seedlings is a major determinant of the lower treeline. Minimum DSI values of 0.28 best predicted presence/absence of forest cover (Table S5), with moderate accuracy (kappa of 0.47 for the entire Bitterroot and 0.65 for the Skalkaho subbasin as compared to Landfire). DSI patterns corresponded to elevation, aspect and convergence influences on forest cover, although there were differences that became apparent when scaling and aggregating the outputs across spatial resolutions, reflecting local influences on forest extent (Fig. S4).

Discussion

Ech2o-SPAC simulates hydraulic response in the glasshouse and predicts seedling mortality in the field

Ech2o-SPAC effectively simulated plant mortality from the glasshouse experiment (Fig. 2) by integrating four factors (Anderegg *et al.*, 2012): intensity, duration, frequency of hydraulic stress and a mortality approach based on point of no return. Therefore, the physical and biological representation of the SPAC as implemented in the model was adequate for simulating soil moisture depletion, ponderosa pine seedling physiological state and mortality. Ech2o-SPAC performed comparably to other physiological models (TREES: Mackay *et al.*, 2015; Tai *et al.*, 2017; MuSICA & ED(X): McDowell *et al.*, 2013).

Studies of post-fire regeneration in western North American coniferous forests consistently show that moisture availability is a major constraint for young seedling survival (Davis *et al.*, 2018). Because of their small size, the buffering capacity of 1-yr-old seedlings is extremely limited and diurnal dynamics of moisture stress are particularly important to capture the effects of duration and frequency of stress in seedlings. Even for adult trees, McDowell *et al.* (2013) found that time over a threshold of stress predicted mortality more effectively than maximum stress levels alone. While nonstructural carbohydrates have also been involved in mortality from hydraulic stress (McDowell, 2011; Sala *et al.* 2012), the focus on hydraulic conductivity is justified in very young seedlings where water transport is critical for photosynthesis and carbon allocation to growth. We found that stress initiates at a PLC of 26% and that the critical threshold for mortality is a PLC of 55%. These values are consistent with those of Adams *et al.* (2017) where mortality events across species occurred at 60% or higher PLC and of McDowell *et al.* (2013) where piñon pine (*Pinus edulis*) surviving drought had a mean PLC of 41%, while those that died had a mean PLC of 63%.

Our modeling framework performed well when scaled from the glasshouse to point simulations across the landscape, capturing population-level mortality as measured on 1-yr-old

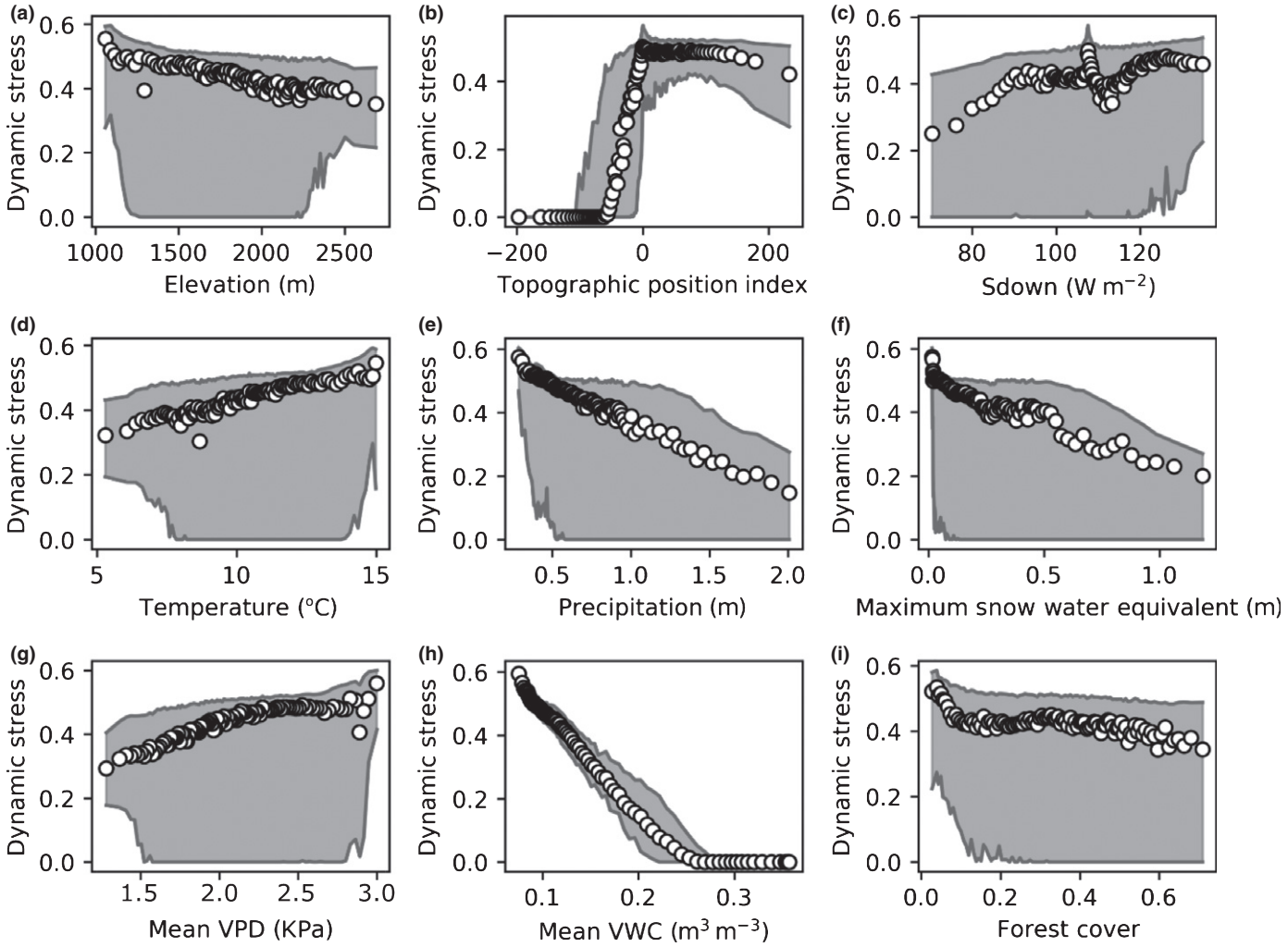

Fig. 6 Relationships between dynamic stress index (DSI) of ponderosa pine seedlings and physical, climatic and ecohydrologic variables. Points are the median DSI values and the gray shaded area represents the 10th and 90th percentile ranges for DSI split into 100 bins based on: (a) elevation, (b) topographic position index, (c) mean solar radiation (Sdown), (d) mean maximum daily temperature (°C), (e) total annual precipitation (m), (f) peak annual snow water equivalent (m), (g) summer mean minimum daily vapor pressure deficit (VPD) (kPa), (h) summer mean volumetric water content (VWC) in the rooting zone, and (i) percentage forest cover derived from MODIS. VWC had the strongest correlation with seedling mortality.

out-planted seedlings (Fig. 3). Such performance is remarkable given that seedlings are usually planted in favorable microsites and mechanisms other than hydraulic stress (e.g. herbivory) may occur in the field. We note that in this application of the model we refrained from additional calibration or adjustments to the parameters, using values from the glasshouse. These two independent applications illustrate the capacity of the model to simulate seedling mortality at multiple spatial scales while accounting for the influence of heterogeneous environmental settings using singly calibrated parameters. Based on our calibration, 17% of the growing season had to surpass the PLC_{crit} threshold for total (100%) mortality in a seedling population. By contrast, but consistent with greater vulnerability in seedlings, Anderegg *et al.* (2015a) found that adult aspen (*Populus tremuloides*) experienced exacerbated mortality after *c.* 30 months of extreme PLC.

Our sensitivity analysis shows that the legacy parameter has a strong effect on the modeled probability of mortality (Fig. S5), indicating that seedlings do not fully recover after a stress event. This sensitivity supports work by L. D. L. Anderegg *et al.* (2013) highlighting the importance of better quantification of plant legacy effects and the results of hydraulic deterioration in predictions of mortality, especially in drier environments (Dorman *et al.*, 2013) and near species range limits (Camarero *et al.*, 2018). These results combined with empirical evidence (Hacke *et al.*, 2001; W. R. L. Anderegg *et al.*, 2013, 2015b) indicate that intensity and duration of stress interact with prior legacy effects to drive mortality (Anderegg *et al.*, 2012) and should be included in simulations of hydraulic stress-induced mortality. The DSI framework quantitatively shows that instantaneous measures of stress are insufficient to describe mortality, and that total stress in a plant is compounded and can be larger than the simple sum of individual events due to legacy effects and accumulated impairment of hydraulic function. When properly calibrated, the DSI allows insight into plant resilience by providing a measure of the relative stress duration at a given intensity required to cause damage that can be compared across species and environments.

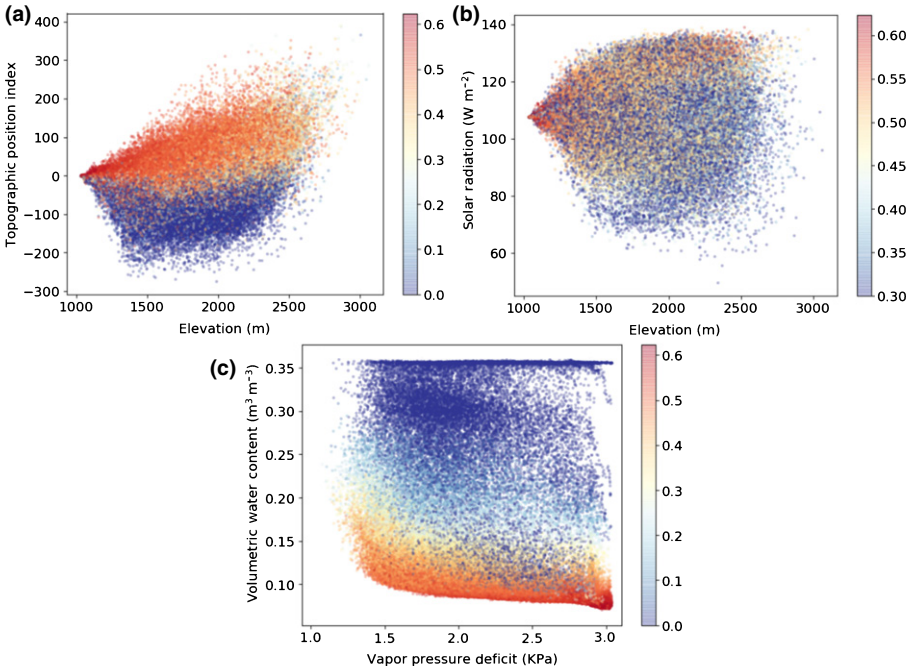

Fig. 7 (a, b) Scatter plots examining how elevation and either topographic position index (TPI) or solar radiation influence dynamic stress index (DSI) in ponderosa pine seedlings. Color corresponds to the average DSI value during the simulated time period according with the color bar on the right side of each figure and each point represents an individual location. For solar radiation this trend is only present at high DSI values (in this case the DSI color scale starts at 0.3. (c) Scatter plot examining the combined influence of vapor pressure deficit and volumetric water content on DSI.

Landscape patterns of stress and mortality

Previous studies examining the relationships between hydraulic stress and tree mortality often use gridded weather inputs at resolutions (> 4 km) that do not either resolve fine-scaled variations in temperature and radiation or account for lateral water routing in complex mountainous terrain. Questions related to tree mortality in complex terrain, however, demand climatic inputs at higher spatiotemporal resolutions and insights into the benefits of potential water subsidies from upslope regions. Tai *et al.* (2017) advanced the simulation of mortality across complex terrain, using a statistical relationship based on static terrain variables to indirectly address the influence of lateral redistribution of water. We build on these advances by integrating the simulation of the SPAC in a spatially distributed, physically based model that simulates the lateral redistribution of water across landscapes and uses gridded datasets that account for climatic variations in aspect at subdaily time steps. The higher radiation loads and 3–4°C differences on south- vs north-facing aspects (Holden *et al.*, 2016) translate into observable differences in DSI with aspect position (Fig. 5). Accounting for topographic variations in energy and moisture resolved at fine resolutions is important to explain observed spatial patterns of mortality and delineate areas with high probability of future die-offs, which is useful to inform forest management. Reforestation specialists understand that landscape position impacts survival and they use topography to select favorable locations for increasing seedling survival (S. Fox, pers. comm.). However, this selection is qualitative and based on experience. Our study demonstrates the potential to integrate complex, mechanistic modeling at a scale that resolves important sources of topographic variation and quantifies seedling mortality risk, which can support localized decision-making.

Patterns of energy, water availability and physiological stress vary significantly across the landscape, highlighting the importance of considering both moisture supply and atmospheric demand when simulating plant stress. An exclusive focus on energy and atmospheric demand for water (VPD) as a proxy for plant stress (Williams *et al.*, 2013) may result in overestimates of stress in valley bottoms and convergent zones. Similarly, focusing only on precipitation or VWC as a proxy for water supply and plant stress (Porporato *et al.*, 2001) may result in overestimates of stress in higher elevation regions. These areas tend to be drier during the summer months because they typically have shallower soils and strong drainage. However, atmospheric demand is lower in these areas, reducing plant stress and water usage.

The DSI from Ech2o-SPAC integrates the balance between water supply and demand on plant vascular hydraulic stress (Fig. 6). Increased available energy increases DSI (Fig 6c,d,g) while increased available water decreases DSI (Fig. 6e,f,h). Low-elevation, south-facing, nonconvergent locations with high atmospheric demand and limited upslope water subsidies had the highest rates of modeled mortality. This is consistent with the topographic positions of documented drought-induced mortality events (Allen & Breshears, 1998; Frey *et al.*, 2004; Worrall *et al.*, 2008). Soil moisture in the rooting zone appeared to be the dominant control on hydraulic stress (Figs 6h, 7c), supporting findings that water availability is a dominant driver of species distributions in semi-arid ecosystems (Crimmins *et al.*, 2011). Topographic convergence increases water availability across elevations (Fig. 7a), thereby reducing the risk of hydraulic stress in areas where it would otherwise be high. Increased hydrologic convergence limits the coupling between plant hydraulic stress and atmospheric conditions and thus buffers these areas from the impacts of hydraulic stress (Fig. 8). Divergent areas, however, lose water in excess of field capacity downslope, making them more

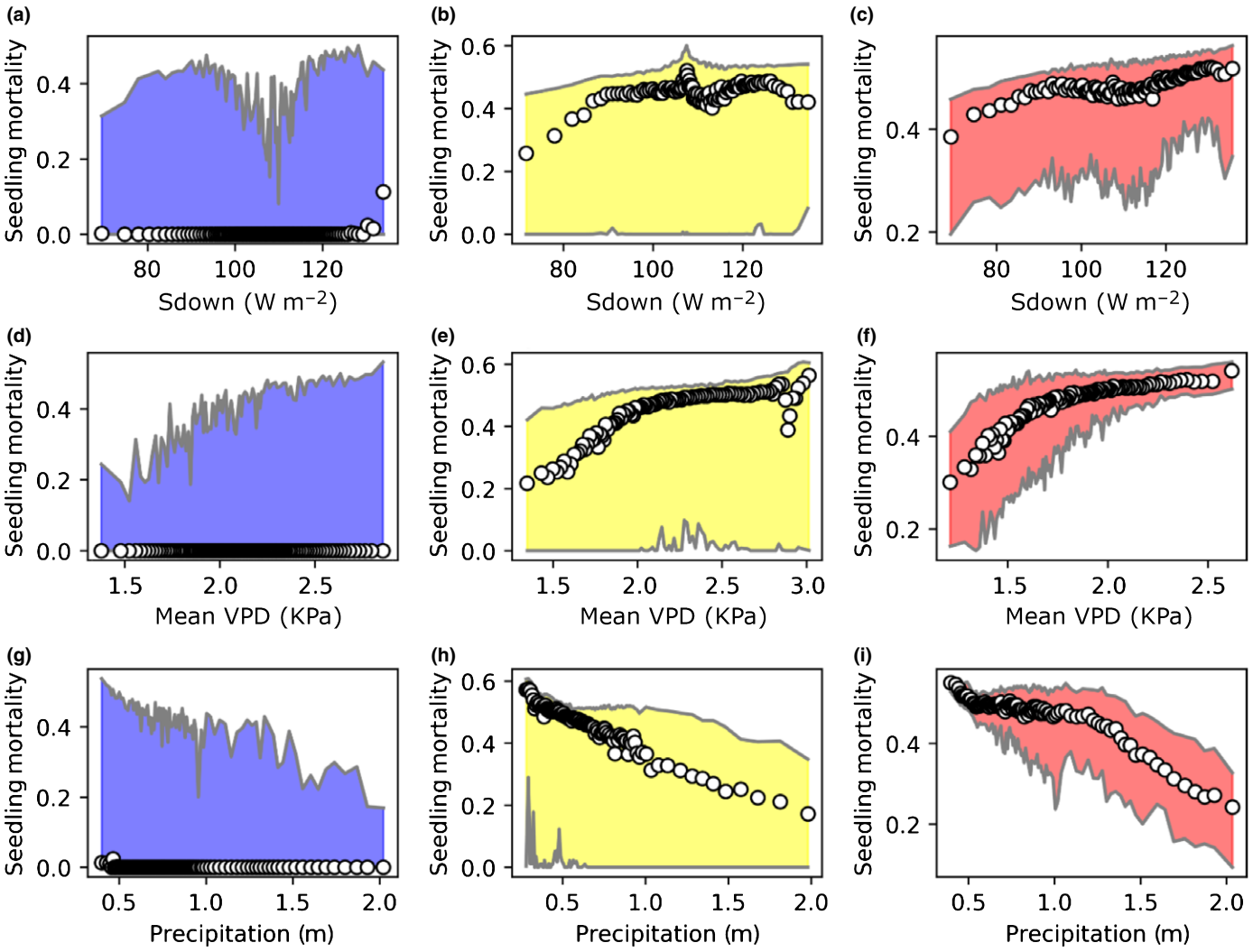

Fig. 8 Relationships between dynamic stress (DSI) in ponderosa pine seedlings and solar radiation (a–c), vapor pressure deficit (d–f) and precipitation (g–i) at different topographic position index values (TPI). The left column (a, d, g) shows relationships for pixels located in convergent areas (TPI values < −50). The middle column (b, e, h) the same for pixels in flat areas (TPI values between −50 and 50). Finally, the right column (c, f, i) shows the relationship for pixels in divergent areas (TPI values > 50). Points are the median dynamic stress values and the gray area is the 10th and 90th percentile range.

tightly coupled and more vulnerable to atmospheric drivers of hydraulic stress.

Hydraulic stress controls on forest distribution

Our simulation of seedling mortality is consistent with the actual distribution of forests near the lower treeline (Fig. 9). Our modeling approach represents conditions consistent with a stand-replacing disturbance as we simulate stresses in the absence of forest canopy. Other factors such as herbivory and dispersal limitation are not accounted for. Observed forest cover is higher at middle to high elevations in the Bitterroot watershed, where simulated seedling mortality is lower. Likewise, DSI is higher and forest cover lower on south-facing slopes than on north-facing slopes, while the reverse is true in riparian corridors and convergent locations. We therefore empirically demonstrate that the distribution of forest cover in our study area corresponds with the simulated distribution of hydraulic stress-induced mortality of 1-yr-old ponderosa pine seedlings. These results suggest that mortality in first-year seedlings is a demographic bottleneck for successful recruitment (Johnson *et al.*, 2011) and that in the absence of other disturbances such as fire, hydraulic stress is a major factor limiting recruitment at the lower treeline in low-elevation coniferous forests of the US Northern Rockies (Barton, 1993; Kroiss & HilleRisLambers, 2015). Minimum stress predicted forest cover better than mean, maximum or median stress (Table S6). This suggests that the least stressful years are the most important for seedling establishment and survival, and that recruitment will be less likely in areas lacking these low-stress years. This is consistent with research showing that ponderosa pine recruitment occurs episodically during cool and wet years (Savage *et al.*, 1996; League & Veblen, 2006).

As water limitations increase, forest mortality is expected to accelerate (Allen *et al.*, 2015; McDowell *et al.*, 2016). Our results suggest that an increase in hydraulic stress will cause an upslope retraction of the lower treeline away from south-facing and

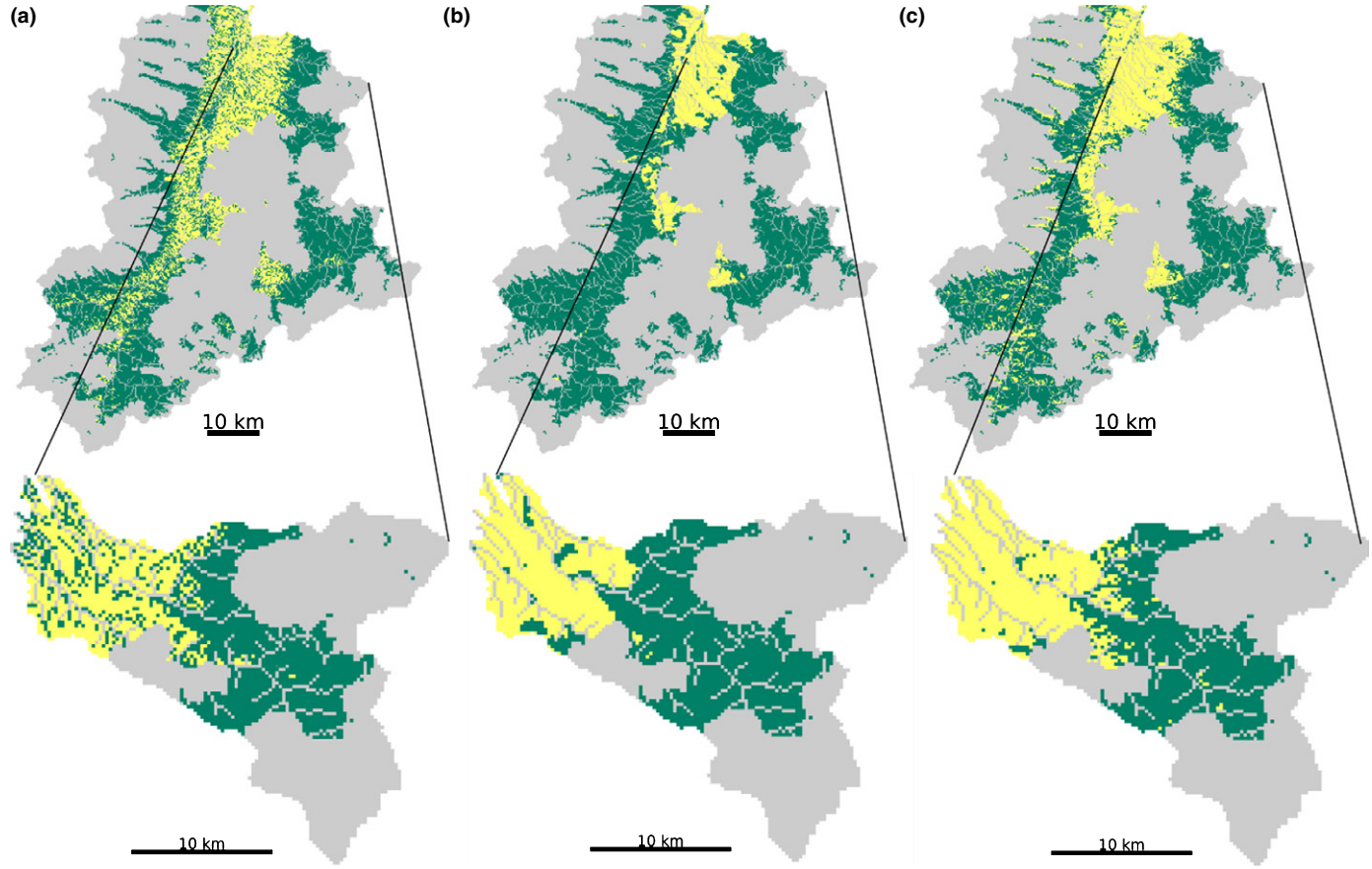

Fig. 9 Maps of forest cover (green) and no forest cover (yellow) in the southern Bitterroot watershed (top) and the Skalkaho catchment (bottom). Gray areas represent streams, locations with < 140 d of growing season (measured by soil temperature over 5°C) to account for the upper treeline, and areas that have been disturbed by fire since 1984. (a) Forest cover predicted from the minimum dynamic stress index (DSI) value at each pixel from 2001 to 2015. Minimum DSI of ponderosa pine seedlings predicted forest cover better than mean, maximum, Q25, median or Q75 (as measured by Cohen's Kappa) (Supporting Information Table S6). Forest cover is predicted where minimum DSI is below 0.28. (b) Actual forest cover from 2015 MODIS percentage cover maps. Actual forest cover is mapped where cover is > 10%. Cohen's Kappa between (a) and (b) is 0.44 for the entire Bitterroot watershed and 0.62 for the Skalkaho catchment. AUC is 0.79 for the Bitterroot and 0.80 for Skalkaho. (c) Forest cover in 2015 measured by Landfire. Cohen's Kappa between (a) and (c) is 0.47 for the entire Bitterroot and 0.65 for the Skalkaho. AUC is 0.75 for the Bitterroot and 0.81 for Skalkaho. Cohen's Kappa between (b) and (c), two independent remotely sensed measures of forest cover, was 0.60 for the entire Bitterroot and 0.79 for the Skalkaho.

nonconvergent areas at moderate risk (Bell *et al.*, 2014). Increases in temperature associated with climate change will probably drive these patterns to some extent, relegating forest to higher elevations and north-facing aspects. Uncertainty of the precipitation response to climate change may complicate this pattern. In western Montana, precipitation is projected to increase in fall, winter and spring, but decrease during the summer (Whitlock *et al.*, 2017). However, the uncertainty in these predictions (Silverman *et al.*, 2013; Silverman & Maneta, 2016; Whitlock *et al.*, 2017) is far greater than the uncertainty of projections of increased temperature. Given that VWC had the strongest relationship with DSI (Figs 6h, 7c), changes in precipitation during the 21st century will probably impact forest distribution. Regardless of the direction of precipitation changes, topographic convergence and lateral routing of water will strongly mediate distributions of hydraulic stress at the lower treeline, further complicating the pattern of upslope directional shifts. Highly convergent areas, often found at lower elevations, will increasingly support isolated pockets of recruitment, thus acting as climate refugia buffering forests from climate change (Dobrowski, 2011; Mclaughlin *et al.*, 2017). Here we build on research showing that abiotic diversity (topographic position and hydrologic routing) buffers ecosystem responses to hydraulic stress (Rodriguez-Iturbe *et al.*, 2009; Bean *et al.*, 2014; Wohl, 2017) and may mitigate some impacts of climate change.

Concluding remarks

We show that a fully integrated ecohydrologic and plant hydraulics model that accounts for spatial heterogeneity in the energy and water balance effectively captured the physiology and mortality of 1-yr-old ponderosa pine seedlings in a glasshouse dry-down experiment. We reasonably simulated observed seedling mortality at sites across western Montana and northern Idaho using an independent data set. These results at multiple spatial scales demonstrate that Ech2o-SPAC is robust under

multiple conditions and suggests that the DSI framework can account for the intensity and duration of hydraulic stress as well as the impact of successive events. Atmospheric and hydrologic controls concentrated simulated seedling mortality at low-elevation, south-facing, nonconvergent locations in the Bitterroot Valley of western Montana. The pattern of this mortality captured current forest cover observations (high simulated seedling mortality corresponds to low forest cover). Our results indicate that increasing hydraulic stress because of global warming may limit seedling recruitment at the lower treeline and reduce the capacity of low-elevation forests to regenerate.

Acknowledgements

This material is based upon work supported by the National Science Foundation under grant no. GSS-1461576. This work was also supported by the National Aeronautics and Space Administration applied sciences program, grant NNH11ZDA001N-FIRES, the USDA National Institute of Food and Agriculture, McIntire Stennis program, project 1012438, and the Institute on Ecosystems Montana NSF EPSCoR. We thank Shelagh Fox and Renate Bush at USFS Region 1 for providing access to stakerow data and Patrick Demaree for assistance with glasshouse data collection.

Author contributions

All authors took part in various pieces of planning and designing the research with SZD leading the planning. GS conducted the glasshouse experiment used in this paper and provided the data for modeling. ZAH acquired the USFS dataset, built climate and soils datasets, and analyzed the data. MPM developed our novel model. CS and MPM conducted the experiment and performed the modeling. CS wrote the manuscript with editorial input from MPM, SZD, ZAH, AS and GS.

ORCID

Zachary A. Holden http://orcid.org/0000-0002-4319-6491
Marco P. Maneta http://orcid.org/0000-0001-6221-0634
Gerard Sapes http://orcid.org/0000-0002-6017-2053
Caelan Simeone http://orcid.org/0000-0003-3263-6452

References

Adams HD, Zeppel MJB, Anderegg WRL, Hartmann H, Landhäusser SM, Tissue DT, Huxman TE, Hudson PJ, Franz TE, Allen CD *et al.* 2017. A multi-species synthesis of physiological mechanisms in drought-induced tree mortality. *Nature Ecology and Evolution* **1**: 1285–1291.

Alden WC. 1953. Physiography and glacial geology of western Montana and adjacent areas. *U.S. Geological Survey Professional Paper* **231**: 1–200.

Allen CD, Breshears DD. 1998. Drought-induced shift of a forest-woodland ecotone: rapid landscape response to climate variation. *Proceedings of the National Academy of Sciences, USA* **95**: 14839–14842.

Allen CD, Breshears DD, McDowell NG. 2015. On underestimation of global vulnerability to tree mortality and forest die-off from hotter drought in the Anthropocene. *Ecosphere* **6**: 292–297.

Allen CD, Macalady AK, Chenchouni H, Bachelet D, McDowell N, Vennetier M, Kitzberger T, Rigling A, Breshears DD, Hogg EH *et al.* 2010. A global overview of drought and heat-induced tree mortality reveals emerging climate change risks for forests. *Forest Ecology and Management* **259**: 660–684.

Anderegg LDL, Anderegg WRL, Berry JA. 2013. Not all droughts are created equal: translating meteorological drought into woody plant mortality. *Tree Physiology* **33**: 701–712.

Anderegg WRL, Berry JA, Field CB. 2012. Linking definitions, mechanisms, and modeling of drought-induced tree death. *Trends in Plant Science* **17**: 693–700.

Anderegg WRL, Flint A, Huang CY, Flint L, Berry JA, Davis FW, Sperry JS, Field CB. 2015a. Tree mortality predicted from drought-induced vascular damage. *Nature Geoscience* **8**: 367–371.

Anderegg WRL, Plavcová L, Anderegg LDL, Hacke UG, Berry JA, Field CB. 2013. Drought's legacy: multiyear hydraulic deterioration underlies widespread aspen forest die-off and portends increased future risk. *Global Change Biology* **19**: 1188–1196.

Anderegg WRL, Schwalm C, Biondi F, Camarero JJ, Koch G, Litvak M, Ogle K, Shaw JD, Shevliakova E, Williams AP *et al.* 2015b. Pervasive drought legacies in forest ecosystems and their implications for carbon cycle models. *Science* **349**: 528–532.

Bailey JD, Harrington C. 2006. Temperature regulation of bud-burst phenology within and among years in a young Douglas-fir (*Pseudotsuga menziesii*) plantation in western Washington, USA. *Tree Physiology* **26**: 421–430.

Barton AM. 1993. Factors controlling plant distributions: drought, competition, and fire in montane pines in Arizona. *Ecological Monographs* **63**: 367–397.

Bean JR, Wilcox AC, Woessner WW, Muhlfeld CC. 2014. Multiscale hydrogeomorphic influences on bull trout (*Salvelinus confluentus*) spawning habitat. *Canadian Journal of Fisheries and Aquatic Sciences* **72**: 514–526.

Beedlow PA, Lee EH, Tingey DT, Waschmann RS, Burdick CA. 2013. The importance of seasonal temperature and moisture patterns on growth of Douglas-fir in western Oregon, USA. *Agricultural and Forest Meteorology* **169**: 174–185.

Bell DM, Bradford JB, Lauenroth WK. 2014. Early indicators of change: divergent climate envelopes between tree life stages imply range shifts in the western United States. *Global Ecology and Biogeography* **23**: 168–180.

Benjaram S, Dixon J. 2015. *Soil chemical weathering under morphologic and climatic controls in the Northern Rockies, Montana.* In: Abstract EP31B-0993 presented at the 2015 Fall Meeting, AGU, San Francisco, CA, USA, December. [WWW document] URL http://adsabs.harvard.edu/abs/2015AGUFMEP31B0993B [accessed 24 April 2018].

Brodribb TJ, Bowman DJ, Nichols S, Delzon S, Burlett R. 2010. Xylem function and growth rate interact to determine recovery rates after exposure to extreme water deficit. *New Phytologist* **188**: 533–542.

Camarero J, Gazol A, Sangüesa-Barreda G, Cantero A, Sánchez-Salguero R, Sánchez-Miranda A, Granda E, Serra-Maluquer X, Ibáñez R. 2018. Forest growth responses to drought at short- and long-term scales in Spain: squeezing the stress memory from tree rings. *Frontiers in Ecology and Evolution* **6**: 1–11.

Choat B, Jansen S, Brodribb TJ, Cochard H, Delzon S, Bhaskar R, Bucci SJ, Feild TS, Gleason SM, Hacke UG *et al.* 2012. Global convergence in the vulnerability of forests to drought. *Nature* **491**: 752–755.

Christensen JH, Hewitson B, Busuioc A, Chen A, Gao X, Held R, Jones R, Kolli RK, Kwon WK, Laprise R *et al.* 2007. Regional climate projections. In: Solomon S, Qin D, Manning M, Chen Z, Marquis M, Averyt KB, Tignor M, Miller HL, eds. *Climate change: The physical science basis. Contribution of Working Group I to the Fourth Assessment Report of the Intergovernmental Panel on Climate Change*. Cambridge, UK and New York, NY, USA: Cambridge University Press.

Cohen J. 1960. A coefficient of agreement for nominal scales. *Educational and Psychological Measurement* **20**: 37–46.

Coops NC, Waring RH, Law BE. 2005. Assessing the past and future distribution and productivity of ponderosa pine in the Pacific Northwest using a process model, 3-PG. *Ecological Modelling* **183**: 107–124.

Crimmins SM, Dobrowski SZ, Greenberg JA, Abatzoglou JT, Mynsberge AR. 2011. Changes in climatic water balance drive downhill shifts in plant species' optimal elevations. *Science* **331**: 324–327.

Daly C, Halbleib M, Smith J, Gibson W, Doggett M, Taylor G, Curtis J, Pasteris P. 2008. Physiographically sensitive mapping of climatological temperature and precipitation across conterminous United States. *International Journal of Climatology.* **28**: 2031–2064.

Daly E, Porporato A, Rodriguez-Iturbe I. 2004. Coupled dynamics of photosynthesis, transpiration, and soil water balance. Part I: Upscaling from hourly to daily level. *Journal of Hydrometeorology* **5**: 546–558.

Davis KT, Higuera PE, Sala A. 2018. Anticipating fire-mediated impacts of climate change using a demographic framework. *Functional Ecology* **32**: 1729–1745.

DiMiceli CM, Carroll ML, Sohlberg RA, Huang C, Hansen MC, Townshend JRG. 2011. *Annual global automated MODIS vegetation continuous fields (MOD44B) at 250 m spatial resolution for data years beginning day 65, 2000–2010, collection 5 percent tree cover*. College Park, MD, USA: University of Maryland.

Dobrowski SZ. 2011. A climatic basis for microrefugia: the influence of terrain on climate. *Global Change Biology* **17**: 1022–1035.

Dobrowski SZ, Swanson AK, Abatzoglou JT, Holden ZA, Safford HD, Schwartz MK, Gavin DG. 2015. Forest structure and species traits mediate projected recruitment declines in western US tree species. *Global Ecology and Biogeography* **24**: 917–927.

Dorman M, Svoray T, Perevolotsky A, Sarris D. 2013. Forest performance during two consecutive drought periods: diverging long-term trends and short-term responses along a climatic gradient. *Forest Ecology and Management.* **310**: 1–9.

Frey BR, Lieffers VJ, Hogg EHT, Landhäusser SM. 2004. Predicting landscape patterns of aspen dieback: mechanisms and knowledge gaps. *Canadian Journal of Forest Research* **1390**: 1379–1390.

Geman S, Geman D. 1984. Stochastic relaxation, Gibbs distributions, and the Bayesian restoration of images. *IEE Transactions on Pattern Analysis and Machine Intelligence* **6**: 721–741.

Hacke UG, Stiller V, Sperry JS, Pittermann J, Mcculloh KA. 2001. Cavitation fatigue, embolism and refilling cycles can weaken the cavitation resistance of xylem. *Plant Physiology* **125**: 779–786.

Hanley AJ, McNeil JB. 1982. The meaning and use of the area under a receiver operating characteristic (ROC) curve. *Radiology* **143**: 29–36.

Harcombe P. 1987. Tree life tables. *BioScience* **37**: 557–568.

Hartmann H, Adams HD, Anderegg WRL, Jansen S, Zeppel MJB. 2015. Research frontiers in drought-induced tree mortality: crossing scales and disciplines. *New Phytologist* **205**: 965–969.

Hastings WK. 1970. Monte Carlo sampling methods using Markov chains and their applications. *Biometrika* **57**: 97–109.

Hawthorne S, Miniat CF. 2018. Topography may mitigate drought effects on vegetation along a hillslope gradient. *Ecohydrology* **11**: 1–11.

Holden ZA, Swanson A, Klene AE, Abatzoglou JT, Dobrowski SZ, Cushman SA, Squires J, Moisen GG, Oyler JW. 2016. Development of high-resolution (250 m) historical daily gridded air temperature data using reanalysis and distributed sensor networks for the US Northern Rocky Mountains. *International Journal of Climatology* **36**: 3620–3632.

Holden ZA, Swanson A, Luce C, Jolly M, Maneta M, Warren A, Oyler J, Parson R, Affleck D. 2018. Decreasing fire season precipitation increase western US wildfire area burned. *Proceedings of the National Academy of Sciences, USA* **155**: E8349–E8357.

Huang M, Wang X, Keenan T, Piao SL. 2018. Drought timing influences the legacy of tree growth recovery. *Global Change Biology* **24**: 3546–3559.

Hubbard RM, Ryan MG, Stiller V, Sperry JS. 2001. Stomatal conductance and photosynthesis vary linearly with plant hydraulic conductance in ponderosa pine. *Plant, Cell & Environment* **24**: 113–121.

IPCC. 2015. Core Writing Team, Pachauri RK, Meyer LA, eds. *Climate change 2014: Synthesis report. Contribution of Working Groups I, II and III to the Fifth Assessment Report of the Intergovernmental Panel on Climate Change*. Geneva, Switzerland: IPCC.

Jiang X, Rauscher SA, Ringler TD, Lawrence DM, Park Williams A, Allen CD, Steiner AL, Michael Cai D, McDowell NG. 2013. Projected future changes in vegetation in western North America in the twenty-first century. *Journal of Climate* **26**: 3671–3687.

Johnson DM, Mcculloh KA, Reinhardt K. 2011. The earliest stages of tree growth: development, physiology and impacts of microclimate. In: Meinzer FC, Lachenbruch B, eds. *Size- and age-related changes in tree structure and function*. Dordrecht, the Netherlands: Springer, 65–90.

Kroiss S, HilleRisLambers J. 2015. Recruitment limitation of long-lived conifers: implications for climate change responses. *Ecological Society of America* **96**: 1286–1297.

Kueppers LM, Conlisk E, Castanha C, Andrew B. 2017. Warming and provenance limit tree recruitment across and beyond the elevation range of subalpine forest. *Global Change Biology* **23**: 2383–2395.

Kuppel S, Tetzlaff D, Maneta MP, Soulsby C. 2018. What can we learn from multi-data calibration of a process-based ecohydrological model? *Environmental Modelling and Software* **101**: 301–316.

Landguth EL, Holden ZA, Mahalovich MF, Cushman SA. 2017. Using landscape genetics simulations for planting blister rust resistant whitebark pine in the US Northern Rocky Mountains. *Frontiers in Genetics* **8**: 1–12.

League K, Veblen T. 2006. Climatic variability and episodic *Pinus ponderosa* establishment along the forest-grassland ecotones of Colorado. *Forest Ecology and Management* **228**: 98–107.

Lozano-Parra J, Maneta MP, Schnabel S. 2014. Climate and topographic controls on simulated pasture production in a semiarid Mediterranean watershed with scattered tree cover. *Hydrology and Earth System Sciences* **18**: 1439–1456.

Luedeling E. 2018. *chillR: Statistical methods for phenology analysis in temperate fruit trees. R package v.0.70.2*. [WWW document] URL https://CRAN.R-project.org/package=chillR [accessed 29 July 2018].

Mackay DS, Ahl DE, Ewers BE, Samanta S, Gower ST, Burrows SN. 2003. Physiological tradeoffs in the parameterization of a model of canopy transpiration. *Advances in Water Resources* **26**: 179–194.

Mackay DS, Roberts DE, Ewers BE, Sperry JS, McDowell NG, Pockman WT. 2015. Interdependence of chronic hydraulic dysfunction and canopy processes can improve integrated models of tree response to drought. *Water Resources Research* **51**: 6156–6176.

Maneta MP, Silverman NL. 2013. A spatially distributed model to simulate water, energy, and vegetation dynamics using information from regional climate models. *Earth Interactions* **17**: 1–44.

Martínez-Vilalta J, Garcia-Forner N. 2017. Water potential regulation, stomatal behavior and hydraulic transport under drought: deconstructing the iso/anisohydric concept. *Plant, Cell & Environment* **40**: 962–976.

McDowell N, Pockman WT, Allen CD, Breshears DD, Cobb N, Kolb T, Plaut J, Sperry J, West A, Williams DG *et al.* 2008. Mechanisms of plant survival and mortality during drought: why do some plants survive while others succumb to drought? *New Phytologist* **178**: 719–739.

McDowell NG. 2011. Mechanisms linking drought, hydraulics, carbon metabolism, and vegetation mortality. *Plant Physiology* **155**: 1051–1059.

McDowell NG, Fisher RA, Xu C, Domec JC, Hölttä T, Mackay DS, Sperry JS, Boutz A, Dickman L, Gehres N *et al.* 2013. Evaluating theories of drought-induced vegetation mortality using a multimodel-experiment framework. *New Phytologist* **200**: 304–321.

McDowell NG, Williams AP, Xu C, Pockman WT, Dickman LT, Sevanto S, Pangle R, Limousin J, Plaut J, Mackay DS *et al.* 2016. Multi-scale predictions of massive conifer mortality due to chronic temperature rise. *Nature Climate Change* **6**: 295–300.

Mclaughlin BC, Ackerly DD, Klos PZ, Natali J. 2017. Hydrologic refugia, plants, and climate change. *Global Change Biology* **26**: 2941–2961.

Mesinger F, DiMego G, Kalnay E, Mitchell K, Shafran PC, Ebisuzaki W, Jović D, Woollen J, Rogers E, Berbery EH *et al.* 2006. North American regional reanalysis. *Bulletin of the American Meteorological Society* **87**: 343–360.

Mitchell PJ, O'Grady AP, Tissue DT, White DA, Ottenschlaeger ML, Pinkard EA. 2013. Drought response strategies define the relative contributions of hydraulic dysfunction and carbohydrate depletion during tree mortality. *New Phytologist* **197**: 862–872.

Moyes A, Castanha C, Germino M, Kueppers L. 2013. Warming and the dependence of limber pine (*Pinus flexilis*) establishment on summer soil moisture within and above its current elevation range. *Oecologia* **171**: 271–282.

Ogée J, Brunet Y, Loustau D, Berbigier P, Delzon S. 2003. MuSICA, a CO_2, water and energy multilayer, multileaf pine forest model: evaluation from hourly to yearly time scales and sensitivity analysis. *Global Change Biology* **9**: 697–717.

Parmesan C, Yohe G. 2003. A globally coherent fingerprint of climate change impacts across natural systems. *Nature* **421**: 37–42.

Pellizzari E, Camarero JJ, Gazol A, Sangüesa-Barreda G, Carrer M. 2016. Wood anatomy and carbon-isotope discrimination support long-term hydraulic deterioration as a major cause of drought-induced dieback. *Global Change Biology* **22**: 2125–2137.

Petrie MD, Bradford JB, Hubbard RM, Lauenroth WK, Andrews CM, Schlaepfer DR. 2017. Climate change may restrict dryland forest regeneration in the 21st century. *Ecology* **98**: 1548–1559.

Petrie MD, Wildeman AM, Bradford JB, Hubbard RM, Lauenroth WK. 2016. A review of precipitation and temperature control on seedling emergence and establishment for ponderosa and lodgepole pine forest regeneration. *Forest Ecology and Management* **361**: 328–338.

Porporato A, Laio F, Ridolfi L, Rodriguez-Iturbe I. 2001. Plants in water-controlled ecosystems: active role in hydrologic processes and response to water stress III. Vegetation water stress. *Advances in Water Resources* **24**: 707–723.

Potter KM, Hipkins VD, Mahalovich MF, Means RE. 2013. Mitochondrial DNA haplotype distribution patterns in *Pinus ponderosa* (*Pinaceae*): range-wide evolutionary history and implications for conservation. *American Journal of Botany* **100**: 1562–1579.

R Core Team. 2010. *R: A language and environment for statistical computing.* Vienna, Austria: R Foundation for Statistical Computing. [WWW document] URL http://www.R-project.org/ [accessed 12 February 2016].

Rehfeldt GE, Jaquish BC, Sáenz-Romero C, Joyce DG, Leites LP, Bradley St Clair J, López-Upton J. 2014. Comparative genetic responses to climate in the varieties of *Pinus ponderosa* and *Pseudotsuga menziesii*: reforestation. *Forest Ecology and Management* **324**: 147–157.

Reinhardt K, Germino M, Kueppers L, Domec JC, Mitton J. 2015. Linking carbon and water relations to drought-induced mortality in *Pinus flexilis* seedlings. *Tree Physiology* **35**: 771–782.

Rodriguez-Iturbe I, Muneepeerakul R, Bertuzzo E, Levin SA, Rinaldo A. 2009. River networks as ecological corridors: a complex systems perspective for integrating hydrologic, geomorphologic, and ecologic dynamics. *Water Resources Research* **45**: 1–22.

Rollins MG. 2009. LANDFIRE: a nationally consistent vegetation, wildland fire, and fuel assessment. *International Journal of Wildland Fire* **18**: 235–249.

Rother MT, Veblen TT, Furman LG. 2015. A field experiment informs expected patterns of conifer regeneration after disturbance under changing climate conditions. *Canadian Journal of Forest Research* **45**: 1607–1616.

Sala A, Woodruf DR, Meinzer FC. 2012. Carbon dynamics in trees: feast or famine?. *Tree physiology* **32**: 764–775.

Salvatier J, Wiecki TV, Fonnesbeck C. 2016. Probabilistic programming in Python using PyMC3. *PeerJ Computer Science* **55**: 1–24.

Savage M, Brown PM, Feddema J. 1996. The role of climate in a pine forest regeneration pulse in the southwestern United States. *Écoscience* **3**: 310–318.

Serra-Maluquer X, Mencuccini M, Martínez-Vilalta J. 2018. Changes in tree resistance, recovery and resilience across three successive extreme droughts in the northeast Iberian Peninsula. *Oecologia* **187**: 1–12.

Sevanto S, McDowell NG, Dickman LT, Pangle R, Pockman WT. 2014. How do trees die? A test of the hydraulic failure and carbon starvation hypotheses. *Plant, Cell & Environment* **37**: 153–161.

Silverman NL, Maneta MP. 2016. Detectability of change in winter precipitation within mountain landscapes: spatial patterns and uncertainty. *Water Resources Research* **52**: 4301–4320.

Silverman NL, Maneta MP, Chen SH, Harper JT. 2013. Dynamically downscaled winter precipitation over complex terrain of the Central Rockies of Western Montana, USA. *Water Resources Research* **49**: 458–470.

Smith WK, Germino MJ, Johnson DM, Reinhardt K. 2009. The altitude of alpine treeline: a bellwether of climate change effects. *Botanical Review* **75**: 163–190.

Sperry JS, Adler FR, Campbell GS, Comstock JP. 1998. Limitation of plant water use by rhizosphere and xylem conductance: results from a model. *Plant, Cell & Environment* **21**: 347–359.

Tai X, Mackay DS, Anderegg WRL, Sperry JS, Brooks PD. 2017. Plant hydraulics improves and topography mediates prediction of aspen mortality in southwestern USA. *New Phytologist* **213**: 113–127.

Tai X, Mackay S, Sperry J, Brooks P, Anderegg WRL, Flanagan L, Rood S, Hopkinson C. 2018. Distributed plant hydraulic and hydrological modeling to understand the susceptibility of riparian woodland trees to drought-induced mortality. *Water Resources Research* **54**: 4901–4915.

Tyree MT. 1997. The Cohesion-Tension theory of sap ascent: current controversies. *Journal of Experimental Botany* **48**: 1753–1765.

Tyree MT, Sperry JS. 1988. Do woody plants operate near the point of catastrophic xylem dysfunction caused by dynamic water stress? Answers from a model. *Plant Physiology* **88**: 574–580.

Van Mantgem PJ, Stephenson NL, Byrne JC, Daniels LD, Franklin JF, Fulé PZ, Harmon ME, Larson AJ, Smith JM, Taylor AH *et al.* 2009. Widespread increase of tree mortality rates in the Western United States. *Science* **323**: 521–524.

Venturas MD, Sperry JS, Hacke UG. 2017. Plant xylem hydraulics: what we understand, current research, and future challenges. *Journal of Integrative Plant Biology* **59**: 356–389.

Walther GR, Post E, Convey P, Menzel A, Parmesan C, Beebee TJC, Fromentin JM, Hoegh-Guldberg O, Bairlein F. 2002. Ecological responses to recent climate change. *Nature* **416**: 389–395.

Weiss A. 2001. *Topographic position and landforms analysis. Poster presentation, ESRI User Conference, San Diego, CA, USA* **64**: 227–245. [WWW document] URL http://www.jennessent.com/downloads/TPI-poster-TNC_18x22.pdf [accessed 13 January 2018].

Weiss JL, Castro CL, Overpeck JT. 2009. Distinguishing pronounced droughts in the southwestern United States: seasonality and effects of warmer temperatures. *Journal of Climate* **22**: 5918–5932.

Whitlock C, Cross W, Maxwell B, Silverman N, Wade AA. 2017. *2017 Montana Climate Assessment.* Bozeman and Missoula, MT, USA: Montana State University and University of Montana, Montana Institute on Ecosystems.

Williams AP, Allen CD, Macalady AK, Griffin D, Woodhouse CA, Meko DM, Swetnam TW, Rauscher SA, Seager R, Grissino-Mayer H *et al.* 2013. Temperature as a potent driver of regional forest drought stress and tree mortality. *Nature Climate Change* **3**: 292–297.

Wohl E. 2017. Connectivity in rivers. *Progress in Physical Geography* **41**: 345–362.

Worrall JJ, Egeland L, Eager T, Mask RA, Johnson EW, Kemp PA, Shepperd WD. 2008. Rapid mortality of *Populus tremuloides* in southwestern Colorado, USA. *Forest Ecology and Management* **255**: 686–696.

Wu X, Liu H, Li X, Ciais P, Babst F, Guo W, Zhang C, Magliulo V, Pavelka M, Liu S *et al.* 2018. Differentiating drought legacy effects on vegetation growth over the temperate Northern Hemisphere. *Global Change Biology* **24**: 504–516.

Supporting Information

Additional Supporting Information may be found online in the Supporting Information section at the end of the article:

Fig. S1 Climate inputs for the glasshouse.

Fig. S2 Modeled and measured hydrographs for the Bitterroot watershed.

Fig. S3 Parameter distributions from the dynamic stress index calibration.

Fig. S4 Scale differences in mapping forest cover.

Fig. S5 Sensitivity of mortality predictions to the legacy effect parameter.

Methods S1 Ech2o model summary.

Methods S2 Ech2o-SPAC extension to Maneta & Silverman (2013).

Notes S1 Comment regarding plant hydraulics.

Notes S2 Comment regarding classification accuracy and Kappa.

Notes S3 Comments regarding the USFS seedling survival dataset.

Table S1 Parameter inputs for Ech2o-SPAC (maps).

Table S2 Parameter inputs for Ech2o-SPAC (species parameter table).

Tables S3 Calibration results for Ech2o-SPAC in the glasshouse.

Table S4 Calibration results for the dynamic stress index.

Table S5 Goodness of fits for various measures of DSI from 2001 to 2015.

Table S6 Parameters for adult vegetation in hydrograph simulations.

Please note: Wiley Blackwell are not responsible for the content or functionality of any Supporting Information supplied by the authors. Any queries (other than missing material) should be directed to the *New Phytologist* Central Office.